Comparison of Calculated and Measured Radiative Fluxes Under Altocumulus and Stratocumulus Cloud Layers

D. Xia, S. K. Krueger and K. Sassen
University of Utah
Salt Lake City, Utah

Introduction

Properly accounting for the effects of clouds on radiative fluxes in numerical models of the atmosphere remains difficult. The difficulty arises from the complexity of the processes that determine macroscopic cloud structure (cloud fraction, height, thickness, and water content) and from the need to know microscopic cloud structure (the constitution, shape, and size of the cloud particles) in order to calculate radiative fluxes.

The problems of macroscopic and microscopic cloud structure can be decoupled and addressed separately. Dynamical models of the atmosphere can be used to predict macroscopic cloud formation processes, and the resulting structure compared to macroscopic cloud observations. Observations of the macroscopic and microscopic structure of clouds can be supplied to a radiative transfer code (RTC) which calculates the radiative fluxes. The latter can then be compared with observations in order to test the RTC.

The U.S. Department of Energy (DOE) Atmospheric Radiation Measurement (ARM) Program has taken just such an approach (Stokes and Schwartz 1994; DOE 1996). The problem of predicting macroscopic cloud structure is being addressed with cloud-resolving models (CRM) and single-column models (SCM), while the problem of calculating radiative fluxes through a cloudy atmosphere with a known distribution of cloud particles is being addressed by the Instantaneous Radiative Flux (IRF) Program.

Our interest is with both altocumulus (Ac) and stratocumulus (Sc) clouds. Ac (Sc) are thin, mid-level (low-level) stratiform clouds consisting of water droplets. These clouds have received little attention from either modelers or observational programs, yet these clouds cover large portions of the earth and significantly affect the radiation fields.

Liu and Krueger (1997) are using a CRM to study the formation of Ac and Sc clouds. Here, we follow the IRF approach and compare calculated and measured broadband solar and infrared (IR) radiative fluxes at the surface below Ac and Sc layers. We have taken a very simple approach. We will evaluate its usefulness and recommend ways to improve it.

Method

In order to determine the effects of Ac and Sc on the radiation, we selected an accurate radiative transfer code to calculate the radiative fluxes. The relevant aspects of this code are described in Fu (1991), Fu and Liou (1992), and Krueger et al. (1995). It is a broadband approach with 6 solar and 12 infrared bands. It is based on the correlated k-distribution method and uses the delta four stream scheme for both the solar and infrared regions of the spectrum. Once effective radius, representing the bulk property of the droplet size distribution, and the liquid water content (LWC), along with the temperature, water vapor mixing ratio, and ozone mixing ratio are given for each layer, radiative transfer calculations can be made to obtain the upward and downward solar and IR fluxes.

We will use the Fu-Liou RTC to calculate the downwelling solar and IR radiative fluxes at the surface below an Ac layer that was observed over the ARM Southern Great Plains (SGP) site during an Intensive Observation Period (IOP) on 24 April 1994, between 18:00 and 24:00 UTC. We will compare the calculated fluxes to the observed fluxes. The same calculations were also made for an overcast Sc case observed at the SGP site on 30 April 1994 between 20:40 and 23:20 UTC.

The Ac (Sc) cloud layer was based about 4000 m (1000 m) above sea level. For the RTC, the atmosphere was divided into several layers. From 6 km to 60 km, the layers were 500 m thick. From the surface (at 0.6 km) to 6 km, the layer thickness was 20 m in the cloud layer (which was located between 4 km and 5 km) and increased to 100 to 500 m above and below the cloud.

We used processed SGP radiosonde data at 21:00 UTC for both the 24 April Ac case and the 30 April Sc case. The resulting soundings have the pressure, temperature, and water vapor mixing ratio for each 200-m layer from the surface to 14 km. Above 14 km, we used the Mid-Latitude Standard Atmosphere (MLSA) values. We also used the MLSA ozone mixing ratio profile.

The LWC profile, which is needed by the RTC, is not measurable by radiosondes. However, at the ARM SGP Cloud and Radiation Testbed (CART), four microwave radiometers (MWRs) have been deployed. One is at the Central Facility near Lamont, Oklahoma. These instruments measure the microwave brightness temperatures at frequencies for which atmospheric water vapor and cloud liquid water are the primary contributors. Using a statistical retrieval method developed by Ed Westwater at the National Oceanic and Atmospheric Administration Environmental Technology Laboratory, Jim Liljegren at Pacific Northwest National Laboratory retrieves integrated water vapor ("precipitable water vapor" or PWV) and integrated cloud liquid ("liquid water path" or LWP) (Liljegren 1994).

Data are collected at 20-second intervals which represent 1-second "snapshots" of the sky/cloud in the field of view of the instrument (5 degrees Full-Width-Half-Maximum).

As for the accuracy of the LWP, the theoretical accuracy of the retrieval for a properly calibrated instrument is about +/- 0.03 mm ($30 g/m^{-2}$). Because of the difficulty of making other direct (or indirect) measurements of LWP, it cannot be said for certain that this is achieved. However, for the PWV, Liljegren's (1994) comparisons with collocated radiosondes for 1993 showed an accuracy of +/- 0.07 cm (clear sky) which equals the theoretical accuracy for the PWV retrieval. The sensitivity is about an order of magnitude better than the accuracy. For LWP, using the 1993 data, the sensitivity was 0.003 mm.

We approximated the LWC profile by assuming that the LWC linearly increases with height from cloud base (where LWC = 0) to cloud top. Figure 1 shows the LWC measured by the Forward Scattering Spectrometer Probe (FSSP) versus height for the Ac case. Each dot represents a 1-second observation. Based on these observations, we set the cloud base height to 3900 m and the cloud top height to 4450 m. From observed LWC observations for the Sc case (not shown), cloud base and cloud top levels were set at 1000 m and 1700 m, respectively.

The LWC at cloud top was then estimated by requiring that the LWP obtained from the assumed linear LWC profile match the LWP retrieved from the Central Facility's MWR.

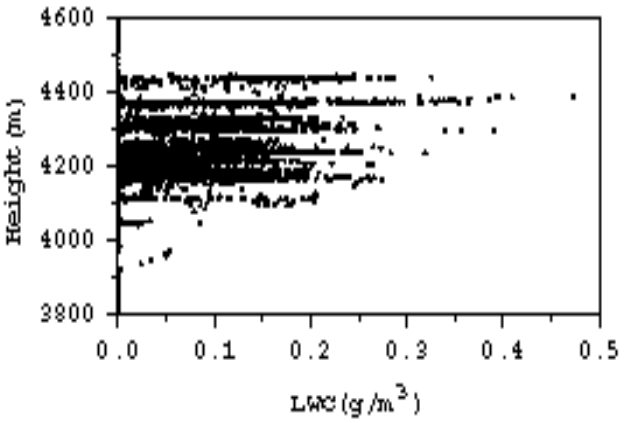

Figure 1. Observed liquid water content versus height from 1 Hz aircraft measurements.

The retrieved LWP was available at 5-minute intervals (as shown in Figures 2 and 7 for Ac and Sc cases, respectively). Also shown is the average LWP determined from the aircraft observations. For both cases, it is roughly half that obtained from the MWR.

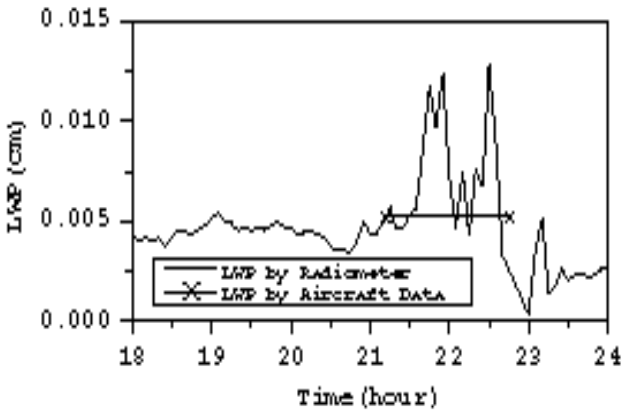

Figure 2. Observed time series of liquid water path from micro-wave radiometer (Ac case).

The effective radius profile is also needed by the RTC. We calculated the effective radius Υ_e at each height from the aircraft FSSP droplet spectrum data using the following formula:

$$\Upsilon_e = \sum_{i=1}^{15} \frac{N_i \Upsilon_i^3}{N_i \Upsilon_i^2} \qquad (1)$$

where N_i is the number concentration of droplets with radius Υ_i.

Figures 3 and 8 show the average effective radius profile in the Ac and Sc layers, respectively. For the Ac (Sc) case, the effective radius increases nearly linearly with height to a maximum of about 7.5 (9.0) microns near cloud top.

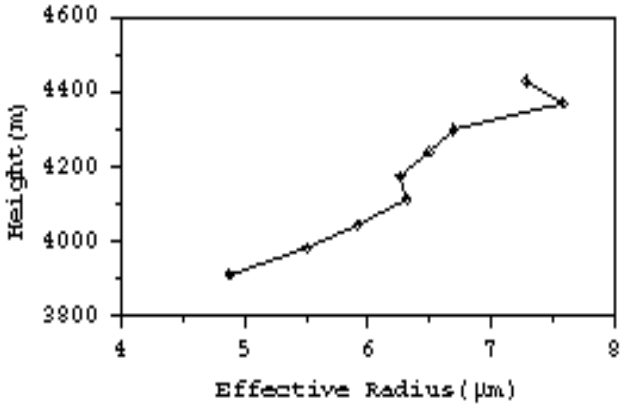

Figure 3. Observed effective radius profile from FSSP aircraft measurements (Ac case).

For partly cloudy conditions, two radiative flux calculations are made: one for a clear sky and one for a cloudy (overcast) sky. These fluxes are then weighted according to the observed clear-sky and cloudy-sky fractions to obtain the total flux. We assume that the MWR LWP values represent cloudy-sky values. An alternative assumption is that they represent a weighted average of clear-sky and cloudy-sky values.

We used ceilometer data to estimate the cloud fraction for the Ac case. The ceilometer at the Central Facility measured the cloud base heights at 1-minute intervals. From these data, we determined the temporal cloud fraction over 1-hour intervals, as shown in Figure 4. The resulting cloud fraction varies from zero to a maximum of about 0.3. For the Sc case, cloud fraction is set to 1.0.

The downwelling solar flux at the top of the atmosphere was obtained using a solar constant of 1365 W m^{-2} and the ratio of the actual to mean earth-sun distance, which depends only on the day of the year. The solar zenith angle was calculated using the site location and the local time.

Results

Ac Case

In Figure 5, we present the following observations and calculations of the downwelling solar flux at the surface:

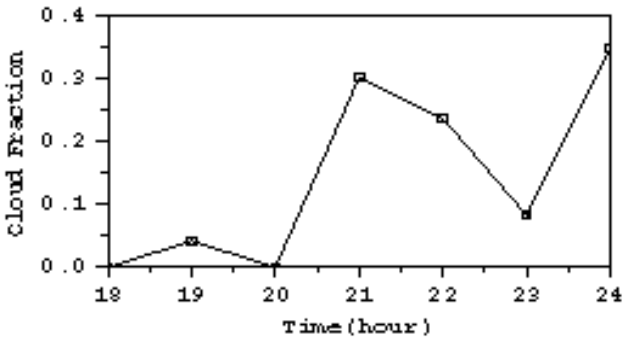

Figure 4. Time series of hourly averaged temporal cloud fraction from ceilometer.

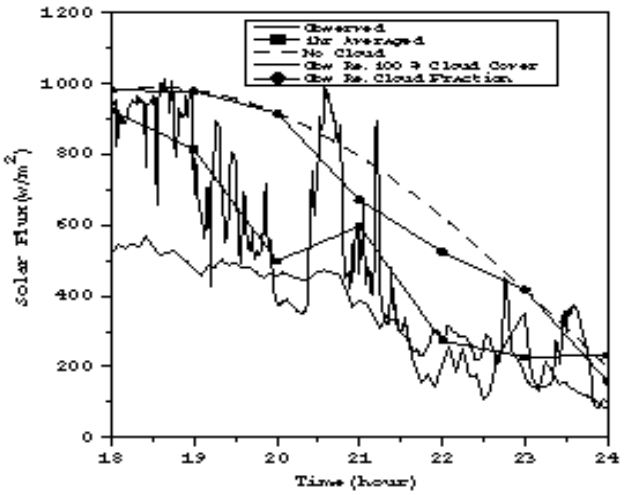

Figure 5. Downwelling solar flux at the surface (Ac case): observed; observed hourly averages; calculated with no clouds: calculated using observed LWP and effective radius with cloud fraction = 1.0; and calculated using observed LWP, effective radius, and ceilometer cloud fraction.

observed; observed hourly averages; calculated with no clouds; calculated using the observed LWP (Figure 2) and effective radius profile (Figure 3) with cloud fraction = 1.0; calculated hourly averages using the LWP, observed effective radius, and ceilometer cloud fraction (Figure 4).

Nearly all of the observed flux values lie between the calculated clear-sky and cloudy-sky values. This is reassuring. Measurements of the direct and diffuse components of the downwelling solar flux at the surface suggest that the periods from 20:00 to 20:30 and 21:30 to 23:30 were mostly cloudy, the periods from 20:30 to 21:00 and 23:30 to 24:00 were mostly clear, and the remaining periods were partly cloudy.

The agreement between calculated cloudy-sky and observed fluxes is good during the cloudy period from 21:30 to 23:30 when the Ac layer was present.

However, the calculated fluxes based on the ceilometer cloud fraction generally exceed the observed fluxes. This could be due to underestimating the cloud fraction and/or the LWP. Satellite and lidar estimates of cloud fraction (obtained from the CERES/ARM/GEWEX[a] [CAGEX] database) are significantly larger than the ceilometer estimates.

Figure 6 shows the same observations and calculations for the downwelling IR flux at the surface. Again, the agreement between calculated cloudy-sky and observed fluxes is good during the cloudy period from 21:30 to 23:30. However, during the 6-hour period, none of the observed values approach the calculated clear-sky values. The use of only one sounding (at 21:00) may contribute to this. It may also be due to the presence of high clouds (indicated by satellite and lidar measurements) during the first part of the period.

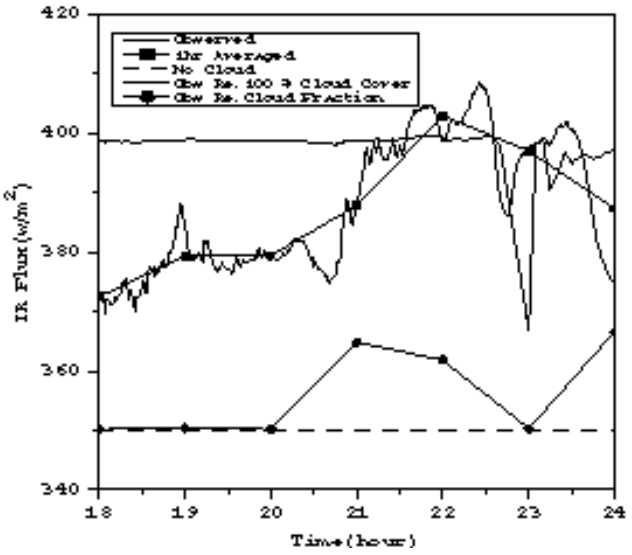

Figure 6. Downwelling infrared flux at the surface (Ac case): observed; observed hourly averages; calculated with no clouds: calculated using observed LWP and effective radius with cloud fraction = 1.0; and calculated using observed LWP, effective radius, and ceilometer cloud fraction.

In addition, the calculated fluxes based on the ceilometer cloud fraction are consistently less than the observed fluxes, which supports the conclusion reached from the solar flux calculations that the ceilometer cloud fraction underestimates the actual cloud fraction.

Sc Case

In Figure 9, we show the observed and calculated downwelling solar flux at the surface for the Sc case. The values obtained from the RTC were calculated using the observed LWP (Figure 7) and the effective radius profile (Figure 8),

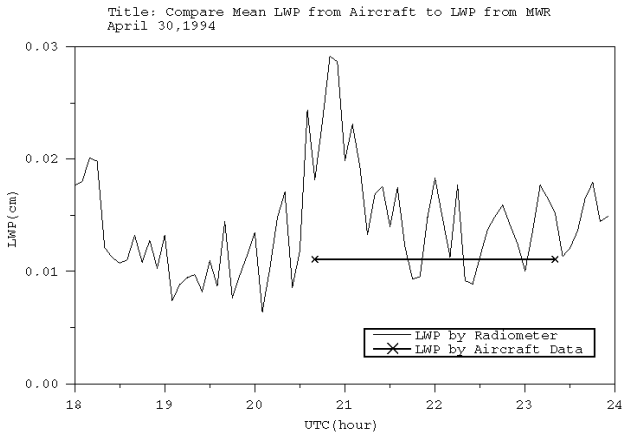

Figure 7. Observed time series of liquid water path from micro-wave radiometer (Sc case).

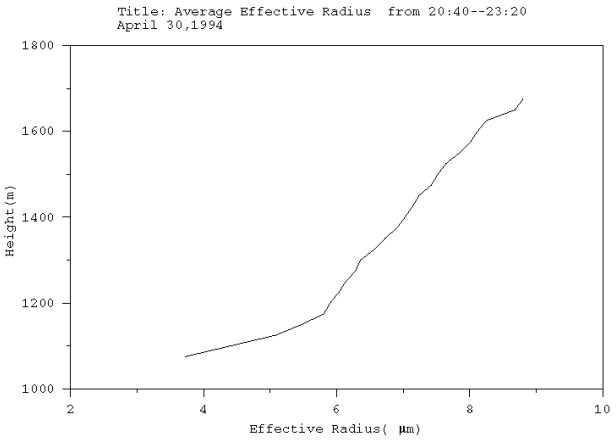

Figure 8. Observed effective radius profile from FSSP aircraft measurements (Sc case).

(a) CERES - Clouds and Earth's Radiant Energy System
GEWEX - Global Energy and Water Experiment

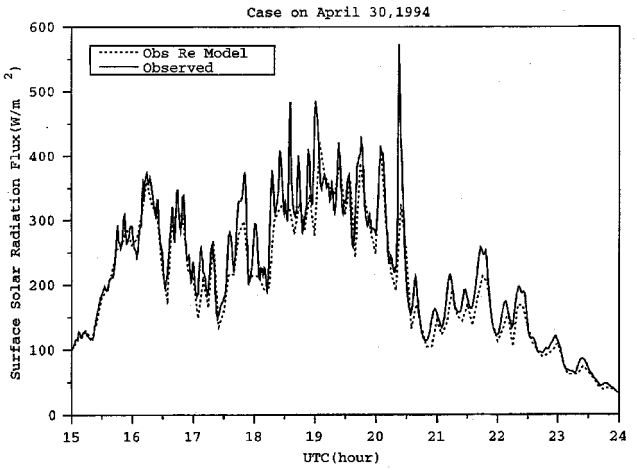

Figure 9. Downwelling solar flux at the surface (Sc case): observed; calculated using observed LWP and effective radius with cloud fraction = 1.0.

assuming a cloud fraction of 1.0. There is good agreement between the calculated cloudy sky and observed fluxes. The calculated fluxes are typically less than the observed, with the largest discrepancies associated with the spikes in the observed upward solar flux after 16 UTC.

The observed and calculated downwelling IR flux at the surface is displayed in Figure 10. Here, too, the agreement is quite good, with differences early in the period on the order of $10\,\mathrm{W\,m^{-2}}$ diminishing to less than $3\,\mathrm{W\,m^{-2}}$ between 21-24 UTC. The calculated IR fluxes are larger than the observed during the entire period.

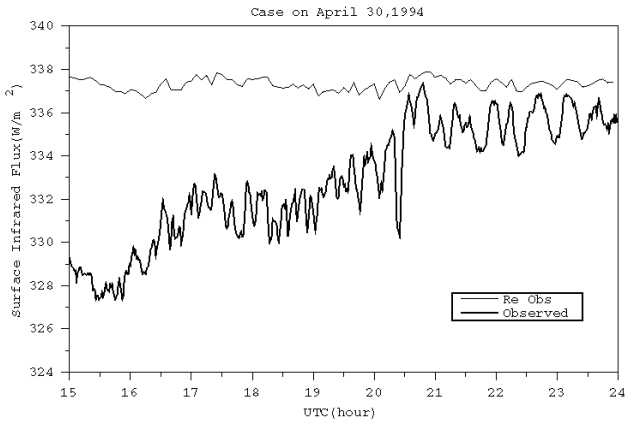

Figure 10. Downwelling infrared flux at the surface (Sc case): observed; calculated using observed LWP and effective radius with cloud fraction = 1.0.

Summary

Good estimates (that is, with errors that are small compared with the differences between the clear-sky and cloudy-sky fluxes) of the downwelling solar and IR fluxes at the surface were obtained during a mostly cloudy period under a layer of Ac. The cloud properties required for the radiative transfer calculations were obtained with a combination of MWR measurements of LWP and aircraft measurements of cloud base height, cloud top height, and effective radius profile. Estimates of the downwelling fluxes based on the ceilometer's temporal cloud fraction were not very good and indicate an underestimate of the actual cloud fraction.

Results indicate that good agreement is obtained between the calculated and measured downward solar fluxes for the overcast Sc case. The agreement between the calculations and observations of the IR flux are reasonable considering that changes in temperature and water vapor were not accounted for in the calculations.

Acknowledgments

This research was supported by the Environmental Science Division, DOE, under Grants DE-FG03-94ER61769 and DE-FG03-94ER61747. The aircraft measurements were supplied by Mike Poellot of the University of North Dakota.

References

Fu, Q., 1991: Parameterization of radiative processes in vertically nonhomogeneous multiple scattering atmospheres. Ph.D. dissertation, Department of Meteorology, University of Utah, Salt Lake City, Utah.

Fu, Q., and K. N. Liou, 1992: On the correlated k-distribution method for radiative transfer in nonhomogeneous atmospheres. *J. Atmos. Sci.*, **49**, 2139-2156.

Krueger, S. K., G. T. McLean, and Q. Fu, 1995: Numerical simulation of the stratus to cumulus transition in the subtropical marine boundary layer. Part I: Boundary layer structure. *J. Atmos. Sci.*, **52**, 2839-2850.

Liljegren, J. C., 1994: Two-channel microwave radiometer for observations of total column precipitable water vapor and cloud liquid water. *Preprints, Fifth Symposium on Global Change Studies*, Nashville, Tennessee, pp. 262-269. American Meteorological Society, Boston, Massachusetts.

Liu, S., and S. K. Krueger, 1997: Effects of radiation in simulated altocumulus cloud layers. *Preprints, Ninth Conference on Atmospheric Radiation*, Long Beach, Calif., American Meteorological Society, Boston, Massachusetts.

Stokes, G. M., and S. E. Schwartz, 1994: The Atmospheric Radiation Measurement (ARM) Program: Programmatic background and design of the Cloud and Radiation Testbed. *Bull. Amer. Meteor. Soc.*, **75**, 1201-1221.

U.S. Department of Energy (DOE), 1996: *Science Plan for the Atmospheric Radiation Measurement Program (ARM)*. DOE/ER-0670T, Washington, D.C.